Limnol. Oceanogr., 55(5), 2010, 2150–2160

doi:10.4319/lo.2010.55.5.2150

Physiological basis for high resistance to photoinhibition under nitrogen depletion in *Emiliania huxleyi*

Martina Loebl,* Amanda M. Cockshutt, Douglas A. Campbell, and Zoe V. Finkel

Environmental Science and Biochemistry, Mount Allison University, Sackville, New Brunswick, Canada

Abstract

We quantified and compared the photophysiological characteristics of *Emiliania huxleyi* with two marine diatoms *Thalassiosira pseudonana* and *Coscinodiscus* sp. under nitrogen- and phosphorus-replete and -depleted conditions. Under nitrogen-depleted conditions, *E. huxleyi* maintained significant photosystem II (PSII) function over at least 38 d, whereas for both diatoms, PSII function declined to marginal levels within 8–10 d of nitrogen depletion. In contrast, under phosphorus-depleted conditions, PSII function in *E. huxleyi* declined sharply within 7 d and in *T. pseudonana* within 3 d. Under nutrient-replete conditions, *E. huxleyi* had one of the highest PSII repair rate constants among phytoplankton examined to date. Under nitrogen depletion, *E. huxleyi* exhibited a decrease in susceptibility to photoinactivation of PSII, while the diatoms showed no significant change in susceptibility. The superior ability of *E. huxleyi* relative to the diatoms to limit PSII photoinactivation as well as to maintain PSII repair for many days of nitrogen depletion could help to explain why *E. huxleyi* is able to form blooms under the low-nitrate, high-light conditions that frequently occur in stratified surface waters.

The cosmopolitan coccolithophore *Emiliania huxleyi* forms globally important blooms that can extend over several thousands of square kilometers (Holligan et al. 1993; Paasche 2002; Raitsos et al. 2006). Often *E. huxleyi* blooms occur after a diatom spring bloom as the water column becomes stratified and macronutrients such as nitrate, phosphate, and silicate are low (Tyrrell and Taylor 1996; Iglesias-Rodríguez et al. 2002). *E. huxleyi* shows no detectable photoinhibition up to light intensities of 1000–1500 μmol photons m^{-2} s^{-1} and in mesocosm experiments outcompetes *Phaeocystis* under high-light conditions, suggesting that this species may have particular physiological capacities to grow under high irradiance (Egge and Heimdal 1994; Nanninga and Tyrrell 1996). Ragni et al. (2008) showed that high-light–adapted *E. huxleyi* cells show faster repair of photoinactivated photosystem II (PSII) than do low-light–adapted cells. The extracellular carbonaceous scales or coccoliths, however, do not seem to act as sunscreen (Nanninga and Tyrrell 1996).

Evidence for nutrient control of *E. huxleyi* blooms is equivocal. *E. huxleyi* has the highest affinity for inorganic phosphorus ever recorded for phytoplankton and can synthesize alkaline phosphatase, which enables it to exploit some organic phosphorus species (Riegman et al. 2000). Furthermore, *E. huxleyi* has been shown to take up organic nitrogen species, such as some amino acids, purines, amides, and urea (Palenik and Henson 1997), although the use of dissolved organic nitrogen differs among *E. huxleyi* strains (Strom and Bright 2009). The uptake of NH_4^+ and urea during blooms has also been reported from field observations in Norwegian fjords and the North Sea (Lessard et al. 2005). Competition experiments of several phytoplankton strains revealed that *E. huxleyi* outcompetes other phytoplankton at high N : P rather than low N : P (Riegman et al. 1992), but *E. huxleyi* blooms have been observed in both low- and high-N : P waters (Tyrrell and Merico 2004). A model study for the northeast Atlantic indicates that low phosphate concentrations in combination with high light are most likely to cause *E. huxleyi* blooms (Tyrrell and Taylor 1996), whereas a model study for the Black Sea found low nitrate concentrations combined with high light most likely to trigger *E. huxleyi* blooms (Oguz and Merico 2006). After examining the environmental conditions associated with several *E. huxleyi* blooms in the North Atlantic and North Sea between 1991 and 1997, Lessard et al. (2005) conclude that most blooms occur in NO_3^--limited waters.

Nitrogen is a key component at the onset of a phytoplankton bloom since autotrophic phytoplankton species use nitrogen for protein synthesis and specifically for the maintenance of the abundant proteins associated with the photosynthetic apparatus. Since PSII reaction centers are constantly damaged by light energy (photoinactivation), cells need nitrogen to synthesize the new proteins required for PSII repair. If PSII repair cannot counteract photoinactivation, for example, because of nitrogen depletion, the cells are subject to photoinhibition (Allakhverdiev and Murata 2004; Nishiyama et al. 2006; Ragni et al. 2008).

No comparison of high-light acclimation between *E. huxleyi* and other phytoplankton such as diatoms has as yet been made under nitrogen-replete and -depleted conditions. We hypothesized that the exceptional high-light adaptation of *E. huxleyi* is based on PSII repair rates (Ragni et al. 2008) that are higher than in other phytoplankton groups and that *E. huxleyi* has a higher capacity to sustain this PSII activity under nitrogen-depleted conditions compared to other dominant phytoplankton groups, such as the diatoms. The following experiments compare photoinactivation rates and counteracting PSII repair rates of *E. huxleyi* to the diatoms *Thalassiosira pseudonana* and *Coscinodiscus* sp. during both nutrient-replete conditions

* Corresponding author: Martina.Loebl@nioz.nl

and nitrogen depletion. $F_V : F_M$ measurements provide a rapid, sensitive, and minimally invasive index for photosynthetic capability (Falkowski and Kolber 1995) and are also a reliable diagnostic of nutrient stress in phytoplankton cultures under unbalanced growth conditions where cells are not adapted to limiting nutrients (Parkhill et al. 2001). As an index of PSII activity, we monitor the progression of maximum quantum yields of PSII ($F_V : F_M$) for all three species during the transition from nutrient repletion to long-term nitrogen and phosphorus depletion.

Methods

Exponential growth—Cultures of *E. huxleyi* (provided by the Alfred Wegener Institute for Polar and Marine Research, Germany, isolated from the North Sea coast at Bergen, Norway), *T. pseudonana*, and *Coscinodicus* sp. (CCMP 1014 and CCMP 1583, both from Provasoli-Guillard National Centre for Culture of Marine Phytoplankton) were grown in semicontinuous batch cultures at 18°C using enriched artificial seawater (ESAW), following Berges et al. (2001), with 549 μmol NO_3 L^{-1}, 21 μmol PO_4 L^{-1}, and 105 μmol Si L^{-1} for all species with pH adjusted to 8.2. Irradiance was $\sim$ 95 μmol photons m^{-2} s^{-1}, provided by white light fluorescence tubes (Sylvania) with a light : dark cycle of 12 : 12 h. Cultures were not stirred or bubbled. Cells were grown under these conditions for at least eight semicontinuous culture transfers over 7–10 wk before experimental treatments were initiated and growth rates were determined. Cell densities were monitored by cell counts using a Beckman coulter counter (Multisizer 3) for *T. pseudonana* and *E. huxleyi* and by Sedwick–Rafter counting chamber under a light microscope for *Coscinodiscus* sp. Growth rates (μ) were estimated from daily countings over several days in five replicate cultures as

$$\mu = \ln(N_t) - \ln(N)/t \quad (1)$$

where N_t is the number of cells at time t (hours) and N the numbers of cells at time zero.

Nitrogen and phosphorus depletion treatments—Cells from five replicate bottles in exponential growth were harvested by gentle filtration using sterile technique onto 0.2-μm polycarbonate filters and transferred into ESAW without nitrogen source (excluding $NaNO_3$) for nitrogen-depleted treatments or into ESAW without phosphorus source for phosphorus-depleted treatments. The iron source of artificial seawater following Berges et al. (2001) is $FeCl_3$ and does not include the $Fe(NH_4)_2(SO_4)$ used in some other ESAW. Pilot surveys verified (via cell counts and $F_V : F_M$ measurements) that cells were transferred successfully, quantitatively, and undamaged. All experimental treatments were maintained in five replicates in 1-liter polycarbonate bottles (Nalgene) and stored at growth conditions described previously (*see* Fig. 1A). The phosphorus depletion experiment was not conducted for *Coscinodiscus* sp. since this experiment functioned mainly as a control to show that results from *E. huxleyi* nitrogen depletion cultures were specific to the physiological response of *E. huxleyi* to nitrogen depletion and not remineralization.

Fluorescence-based maximum quantum yield for PSII ($F_V : F_M$)—We monitored $F_V : F_M$ daily during exponential growth and nutrient depletion treatments. $F_V : F_M$ was measured around the same time in the morning ($\sim$ 3 h after the light turned on in the incubators) from a 2-mL sample of culture, dark adapted for 5 min, using a Xenon Pulse-Amplitude-Modulation (PAM) fluorometer (Walz) in combination with a water-cooled cuvette holder, set to 18°C (Walz). The modulated measuring light beam was set to 4 Hz and the saturating light pulse to 4000 μmol photons m^{-2} s^{-1}. $F_V : F_M$ was calculated as

$$F_V : F_M = (F_M - F_0)/F_M \quad (2)$$

where F_0 was the basal fluorescence at modulated light and F_M the maximum fluorescence at saturating light (Table 1).

Functional absorption cross section—The functional absorption cross section of PSII (σ_{PSII} nm^2 $PSII^{-1}$) for blue light was determined daily at around the same time in a 2-mL culture subsample that was dark adapted for 5 min, using a Fluorescence Induction and Relaxation (FIRe) fluorometer (Satlantic). We applied a 100-μs single-turnover flash given by a blue light-emitting diode (455 $\pm$ 2 nm). The fluorescence rise was analyzed using FIReWORX software (Copyright © 2007 Audrey B. Barnett). Absolute values of σ_{PSII} were determined according to the flash irradiance calibration factor provided by Satlantic. $F_V : F_M$ data resulting from the FIRe were in the range of $F_V : F_M$ data given by the Xenon PAM, but we used the FIRe for σ_{PSII} measurements only and the Xenon PAM for daily $F_V : F_M$ determinations since fluorescence measurements during the light challenge experiments had to be done by the Xenon PAM to determine $F_{M'}$, F_s, and F_0 (described later), but the Xenon PAM is not appropriate to determine σ_{PSII}.

Pigment analysis—Twenty-five milliliters of culture were sampled during exponential growth and in the middle and end of nutrient depletion treatments on 25-mm Millipore filters without binder resin (APFF). Filters were flash frozen in liquid nitrogen and then stored at −80°C. For chlorophyll *a* (Chl *a*) and chlorophyll *c* analysis, pigments were extracted in 90% acetone (saturated with $MgCl_2$) for 18 h at 5°C. Absorption was measured spectrophotometrically following the protocol of Jeffrey and Humphrey (1975).

C : N analysis—For C : N analysis, 13-mm glass-fiber filters were precombusted at 420°C for 6 h. Thirty-milliliter aliquots were sampled with gentle filtration during exponential growth conditions and at several time points during nutrient depletion. After sampling, filters were immediately stored at −80°C. Before they were analyzed, filters were dried at 60°C for 48 h and stored in tin capsules. Prior to analysis, *E. huxleyi* filters were fumed with concentrated HCl for 1 h to remove inorganic carbon

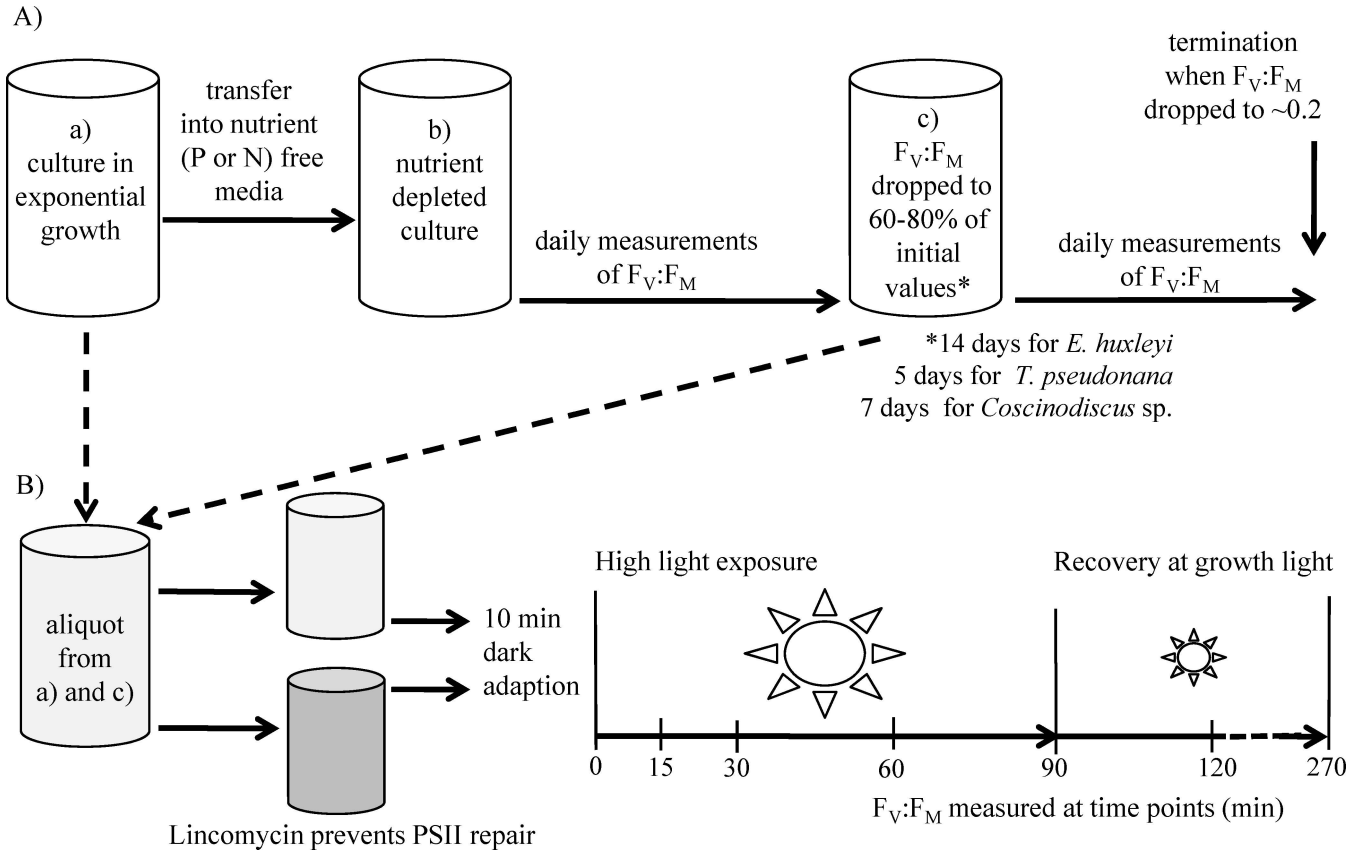

Fig. 1. Schematic overview of (A) the experimental design of nutrient depletion treatments; (B) the experimental design of light challenge experiments.

(Sciandra et al. 2003). Nitrogen and carbon concentrations were analyzed by an elemental analyzer (Vario EL III CHNOS Elementar).

Quantitation of proteins by immunoblotting—For protein quantitations, 100 mL of culture sample were harvested onto 25-mm Millipore APFF filters, once during exponential growth and twice during the nutrient depletion treatment, at the midpoint when $F_V : F_M$ had dropped to 60–80% of initial nutrient-replete values and at the end of the experiment. Filters were flash frozen in liquid nitrogen and then stored at −80°C. Immunoblotting was performed following the protocol of Six et al. (2008) for PsbA (D1 PSII core subunit; Agrisera).

Table 1. List of abbreviations.

μ	Growth rate (d^{-1})
F_0	Basal fluorescence under modulated light
F_M	Maximum fluorescence
F_V	Variable fluorescence (F_M-F_0)
$F_V : F_M$	Fluorescence-based maximum quantum yield of PSII
PSII	Photosystem II
PsbA	Reaction center protein D1 of PSII
R_{PSII}	Repair rate constants of PSII (s^{-1})
σ_{PSII}	Effective absorbance cross section of PSII (nm^2 $PSII^{-1}$)
σ_i	Functional target size for photoinactivation of PSII (nm^2 $PSII^{-1}$)
ETR	Electron transport rates (e^- Chl a^{-1} s^{-1})
DCMU	3-(3,4-dichlorophenyl)-1,1-dimethylurea, inhibitor of the electron transport from PSII to PSI

Electron transport rates (ETR) expressed in e^- Chl a^{-1} s^{-1} were estimated as

$$\mathrm{ETR} = (\mathrm{PSII\ cell}^{-1}) \times \sigma_{\mathrm{PSII}} \times I \times (\mathrm{cell\ Chl}\ a^{-1}) \times \mathrm{qp} \times (4\ \mathrm{electrons}/4\ \mathrm{photons}) \quad (3)$$

where PSII $cell^{-1}$ was estimated from PsbA $cell^{-1}$, σ_{PSII} was the functional absorption cross section in m^2 $PSII^{-1}$, I was the irradiance under nutrient-replete and nitrogen-depleted growth conditions (5.7×10^{19} photons m^{-2} s^{-1}), and the fraction of PSII open and ready to perform photochemistry estimated from qp was calculated as $(F_{M'} - F_S)/(F_{M'} - F_{0'})$. Open PSII use four incoming photons delivered through the functional absorption cross section to photooxidize two molecules of water and pass the resulting four electrons into the electron transport chain.

High-light challenge experiments—In order to estimate PSII repair rate constants (R_{PSII} s^{-1}) and the susceptibility of PSII to photoinactivation (σ_i), parameterized as an effective target size (nm^2 $PSII^{-1}$), high-light challenge experiments were conducted for all species under nutri-

ent-replete conditions and under nitrogen depletion when $F_V : F_M$ dropped to 60–80% of initial values. Figure 1B shows a schematic overview of the experimental design and time course. The high-light challenge experiments were performed following the protocol of Six et al. (2009): subsamples of the culture were split into two flasks, with 500 μg mL^{-1} lincomycin added to one flask to block chloroplast protein synthesis (Bachmann et al. 2004), thereby inhibiting PSII repair (Tyystjarvi and Aro 1996). Both flasks (lincomycin treatment and control treatment without lincomycin) were dark incubated for 10 min to allow the lincomycin to block protein synthesis and then placed at 18°C under 450 μmol photons m^{-2} s^{-1} of blue light for 90 min. Blue light partially mimics a typical marine light field and provokes efficient PSII photoinactivation (Hakala et al. 2005).

At each sampling point t_{min} (after 15, 30, 60, and 90 min of high-light exposure and then after 30 and 180 min of recovery at initial growth light), an aliquot of culture was dark adapted for 5 min. A modulated beam (4 Hz) was used to measure F_0, followed by a saturating white-light pulse (4000 μmol photons m^{-2} s^{-1}) to measure F_M (dark). Actinic light was then administered (450 μmol blue photons m^{-2} s^{-1}), and F_S, the steady fluorescence level in a light-acclimated sample, was measured. A second saturating light pulse was then applied to measure maximal fluorescence in the light ($F_{M'}$). Actinic light was then turned off for a few seconds in order to record the basal level of fluorescence in the light-acclimated sample ($F_{0'}$). Finally, 1 μmol L^{-1} of the PSII inhibitor 3-(3,4-dichlorophenyl)-1,1-dimethylurea (DCMU) was added, and once a steady state was achieved, a final light pulse was triggered to determine the F_M (DCMU) with linear electron transport blocked. Following the light challenge experiments, cultures were returned to their initial growth light of 95 μmol photons m^{-2} s^{-1} for recovery.

PSII repair rate constants were calculated as the differences between the exponential decay of $F_V : F_M$ in the control treatment from t_{15} to t_{90} and the exponential decay in the lincomycin treatment from t_0 to t_{90}. Any initial decline in $F_V : F_M$ during the first 15 min of high-light treatments was corrected by the magnitude of any increase in $F_V : F_M$ during recovery in the culture fraction treated with lincomycin to separate photoinactivation from any influence of nonphotochemical quenching that was sustained during the dark acclimation period before measurement of $F_V : F_M$. The effective target size for PSII photoinactivation (σ_i) (nm^2 PSII^{-1}) was estimated as the exponential decay for $F_V : F_M$ (t_0–t_{90}) in the absence of PSII repair (lincomycin treatment) plotted vs. cumulative photon dose incident on the culture (Allakhverdiev and Murata 2004; Nishiyama et al. 2006; Six et al. 2007). PSII cell^{-1} s^{-1} that were inactivated at the growth light of 95 μmol photons m^{-2} s^{-1} were estimated as

$$\text{PSII cell}^{-1}\ \text{s}^{-1} = \sigma_i \times I \times \text{PSII cell}^{-1} \quad (4)$$

where σ_i was the effective target size for photoinactivation (m^2 quanta^{-1}), I was the experimental irradiance (5.7×10^{19} photons m^{-2} s^{-1}), and PsbA D1 protein content (cell^{-1}) was used as proxy for the content of PSII complexes (Burns et al. 2006).

Results

Growth rates—During exponential growth, the growth rate μ (d^{-1} ± SD, $n = 5$; all abbreviations summarized in Table 1) was 0.75 (± 0.07) for *E. huxleyi*, 0.74 (± 0.03) for *T. pseudonana*, and 0.4 (± 0.07) for *Coscinodiscus* sp. In nitrogen-free media, cell numbers mL^{-1} of all species increased for several days and then remained constant (Table 2).

Fluorescence-based maximum quantum yield for PSII—Before nutrient depletion treatments started, average fluorescence-based maximum quantum yields for PSII ($F_V : F_M$) (± SD, $n = 5$) were 0.57 (± 0.01) for *E. huxleyi*, 0.62 (± 0.03) for *T. pseudonana*, and 0.63 (± 0.01) for *Coscinodiscus* sp. (Fig. 2A) during nutrient-replete growth. $F_V : F_M$ in *E. huxleyi* cultures decreased to values of ~ 0.45 within the first 7 d of nitrogen depletion but then stabilized at this level for another 10 d before values dropped slowly to ~ 0.3 by days 35–38, when the experiment was terminated. For the diatoms, $F_V : F_M$ dropped within 7–10 d of nitrogen depletion to ~ 0.17 in *T. pseudonana* and to ~ 0.24 in *Coscinodiscus* sp. (Fig. 2A). Because of operator error or holidays, some data points result from $n = 4$. In response to phosphorus depletion, $F_V : F_M$ in *E. huxleyi* decreased to ~ 0.24 within 7 d and in *T. pseudonana* to ~ 0.21 within 3 d (Fig. 2B).

Cell content of carbon, nitrogen, Chl a*, Chl* c*, and PsbA*—A summary of Chl *a* cell^{-1}, Chl *c* cell^{-1}, and PsbA cell^{-1} under nutrient-replete and nutrient-depleted conditions is given in Table 2. Nitrogen content per cell decreased in all species investigated, according with the decrease expected by dilution through cell division. Both carbon accumulation and nitrogen dilution through cell division contributed to increasing C : N ratios over the time course of nitrogen depletion treatments (Fig. 2C; Table 2). Under nutrient-replete conditions, *E. huxleyi* contained 0.14 (± 0.04) pg Chl *a* cell^{-1} (average ± SD, $n = 5$) (Fig. 2D) and contained 0.01 (± 0.01) pg Chl *a* cell^{-1} after 38 d of nitrogen depletion. *T. pseudonana* cells contained 0.29 (± 0.04) pg Chl *a* cell^{-1} under nutrient-replete conditions and 0.04 (± 0.01) pg Chl *a* cell^{-1} after 7 d of nitrogen depletion. *Coscinodiscus* sp. contained 96 (± 20) pg Chl *a* cell^{-1} under nutrient-replete conditions and 34 (± 8.2) pg Chl *a* cell^{-1} after 11 d of nitrogen depletion. In combination with decreasing Chl *a* cell^{-1} concentrations, C : Chl *a* ratios (μg cell^{-1}/μg cell^{-1}; ± SD) increased during nitrogen depletion treatments from 41 (± 13) to 838 (± 375) for *E. huxleyi*, from 19 (± 3) to 193 (± 126) for *T. pseudonana*, and from 19 (± 3) to 232 (± 83) for *Coscinodiscus* sp. (Table 2).

The number of PsbA complexes cell^{-1} (± SD, $n = 5$) under nutrient-replete growth conditions was 5.7×10^5 (± 1.9×10^5) for *E. huxleyi*, 7.6×10^5 (± 1.5×10^5) for *T.*

Table 2. Growth rates (d^{-1}), the increase of cell numbers due to cell divisions under nitrogen depletion, cell contents of Chl *a* (pg $cell^{-1}$), Chl *c* (pg $cell^{-1}$), Chl *a*: Chl *c* molar ratios, C: Chl *a* ratios (μg: μg), PSII reaction center D1 protein content (PsbA complexes $cell^{-1}$), and C and N content (μg $cell^{-1}$) under nutrient-replete conditions and under nitrogen depletion. The cell contents of Chl *a*, PsbA, C, and N expected after simple dilution through cell division during nitrogen depletion are given for comparison with measured contents under nitrogen depletion.

			Cells		Chl *a*		Chl *c*	Chl *a*: Chl *c*	Carbon: Chl *a*	PsbA		Carbon		Nitrogen	
Treatment	Day		Growth rate d^{-1}	Fold increase in cells	pg $cell^{-1}$	pg $cell^{-1}$ expected	pg $cell^{-1}$	mol : mol	μg : μg	PsbA $cell^{-1}$	PsbA $cell^{-1}$ expected	μg $cell^{-1}$	μg $cell^{-1}$ expected	μg $cell^{-1}$	μg $cell^{-1}$ expected
E. huxleyi															
Exponential growth		Mean	0.75		0.14		0.04	2.2	41	5.7×10^{5}		6.5×10^{-6}		6.2×10^{-7}	
		±SD	0.07		0.04		0.01	0.2	13	1.9×10^{5}		1.9×10^{-6}		2.6×10^{-7}	
Nitrogen depletion	14	Mean		1.9	0.03	0.08	0.01	1.0	441	9.7×10^{4}	3.4×10^{5}	1.5×10^{-5}	4.1×10^{-6}	3.5×10^{-7}	4.0×10^{-7}
		±SD		0.7	0.01	0.04	0.00	0.3	149	3.0×10^{4}	$1.6.\times10^{5}$	4.0×10^{-6}	2.5×10^{-6}	1.4×10^{-7}	2.7×10^{-7}
Nitrogen depletion	38	Mean		1.8	0.01	0.1	0.01	1.6	838	5.9×10^{4}	3.8×10^{5}	1.1×10^{-5}	4.4×10^{-6}	2.1×10^{-7}	4.4×10^{-7}
		±SD		0.8	0.01	0.04	0.00	0.5	375	1.8×10^{4}	2.1×10^{5}	1.5×10^{-6}	2.3×10^{-6}	7.1×10^{-8}	3.0×10^{-7}
T. pseudonana															
Exponential growth		Mean	0.74		0.29		0.04	5.7	19	7.6×10^{5}		5.5×10^{-6}		1.4×10^{-6}	
		±SD	0.03		0.04		0.01	1.2	3	1.5×10^{5}		6.8×10^{-7}		7.1×10^{-7}	
Nitrogen depletion	5	Mean		3.2	0.08	0.09	0.01	4.2	81	1.4×10^{5}	2.5×10^{5}	6.3×10^{-6}	1.8×10^{-6}	5.0×10^{-7}	4.6×10^{-7}
		±SD		1.2	0.03	0.02	0.00	2.2	32	3.7×10^{4}	7.2×10^{4}	3.1×10^{-6}	4.6×10^{-7}	1.8×10^{-7}	2.3×10^{-7}
Nitrogen depletion	7	Mean		3.2	0.04	0.09	0.01	3.0	193	8.3×10^{4}	2.5×10^{5}	5.4×10^{-6}	1.8×10^{-6}	3.4×10^{-7}	4.6×10^{-7}
		±SD		1.2	0.01	0.02	0.01	1.8	126	6.3×10^{3}	7.2×10^{4}	2.5×10^{-6}	4.6×10^{-7}	9.1×10^{-8}	2.3×10^{-7}
Coscinodiscus sp.															
Exponential growth		Mean	0.39		96.1		13.4	4.9	42	3.4×10^{7}		3.9×10^{-3}		9.3×10^{-4}	
		±SD	0.07		19.9		1.4	0.6	4	8.7×10^{6}		1.1×10^{-3}		2.6×10^{-4}	
Nitrogen depletion	7	Mean		1.4	53.6	70	7.5	5.1	114	<detection limit	2.6×10^{7}	6.4×10^{-3}	2.9×10^{-3}	5.7×10^{-4}	6.9×10^{-4}
		±SD		0.2	10.8	9.8	2.7	1.3	37		6.2×10^{6}	1.2×10^{-3}	5.9×10^{-4}	1.4×10^{-4}	1.0×10^{-4}
Nitrogen depletion	11	Mean		1.4	34.3	68	5.5	4.9	232	<detection limit	2.6×10^{7}	7.3×10^{-3}	2.8×10^{-3}	6.5×10^{-4}	6.5×10^{-4}
		±SD		0.2	8.19	12.3	2.4	2.3	83		6.2×10^{6}	1.6×10^{-3}	6.8×10^{-4}	8.6×10^{-5}	1.1×10^{-4}

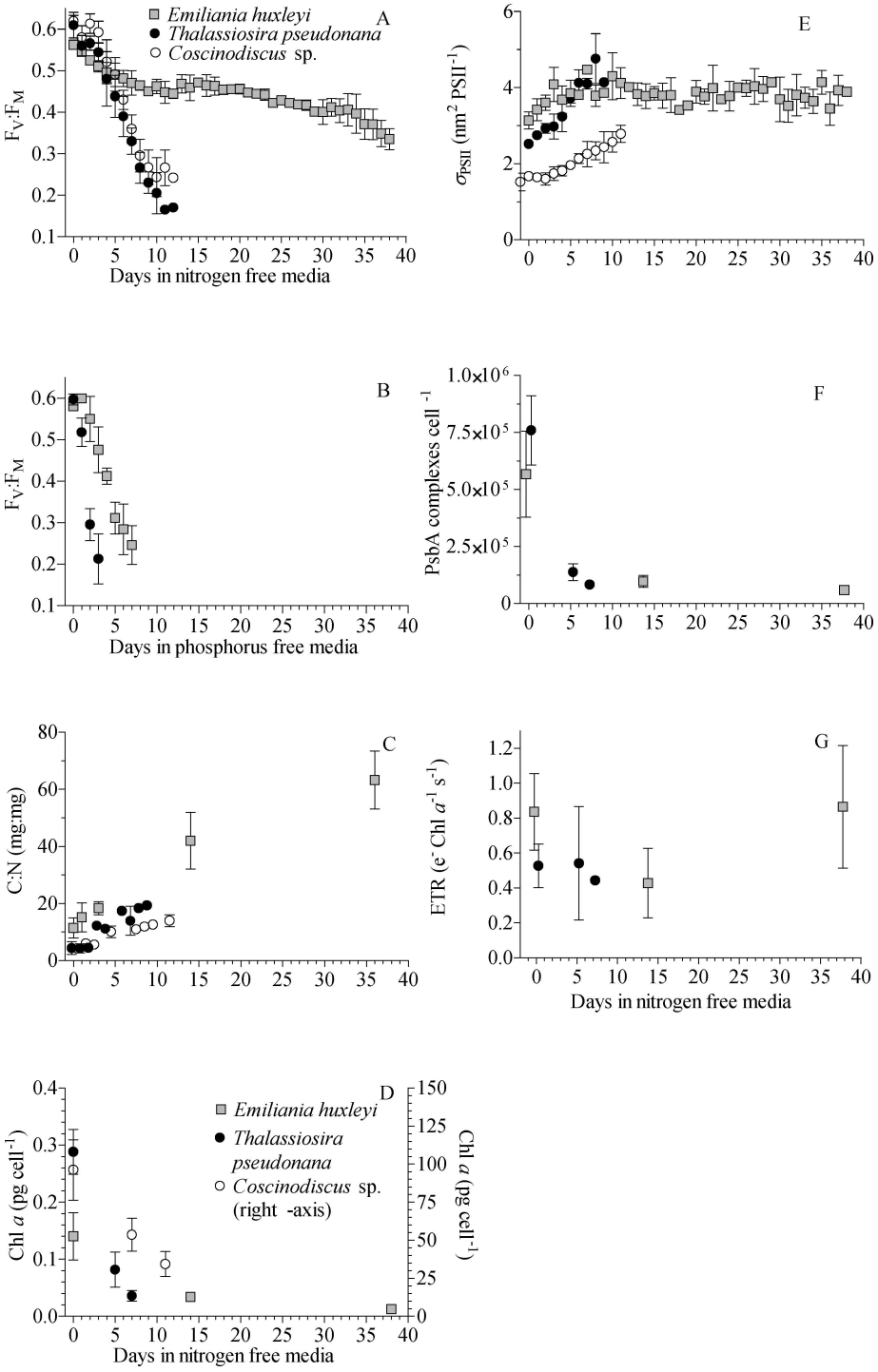

Fig. 2. Time course of the fluorescence-based average maximum quantum yields of PSII ($F_V : F_M$) for *E. huxleyi*, *T, pseudonana*, and *Coscinodiscus* sp. during (A) nitrogen depletion (n = 5, ± SD); (B) phosphorus depletion (n = 3, ± SD); (C) C : N ratios (g : g) (n = 3, ± SD) during nitrogen depletion; (D) cellular Chl *a* (pg cell^{-1}), (n = 3, ± SD) during nitrogen depletion; (E) functional absorbance cross section of PSII (nm^2 PSII^{-1}) for *E. huxleyi*, *T. pseudonana*, and *Coscinodiscus* sp. (n = 4, ± SD) during nitrogen depletion; (F) cellular PsbA (PsbA protein cell^{-1}) (n = 5, ± SD) during nitrogen depletion; and (G) electron transport rates (ETR, e$^-$ Chl a^{-1} s^{-1}) (n = 5, ± SD) during nitrogen depletion for *E. huxleyi* and *T. pseudonana*. Data for *Coscinodiscus* sp. are not presented in (F, G) since PsbA protein levels dropped below the detection limit during nitrogen starvation so that no comparison between nitrogen-replete and nitrogen-depleted conditions was possible.

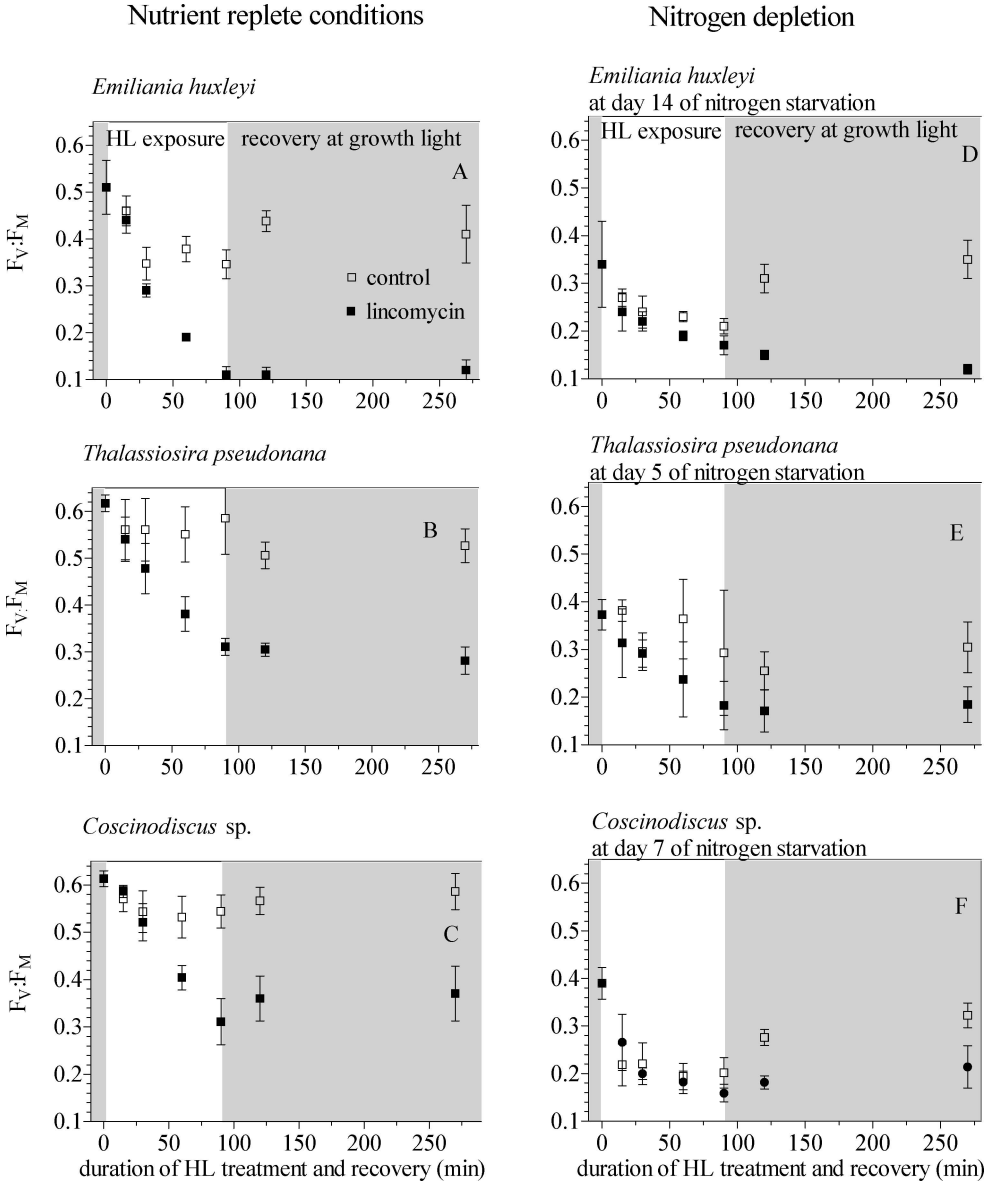

Fig. 3. Maximum quantum yields of PSII ($F_V : F_M$) during 90-min light challenge experiments and the following 180-min recovery phase for control and lincomycin (absence of PSII repair) treatments of (A, D) *E. huxleyi* (n = 4, ± SD), (B, E) *T. pseudonana* (n = 5, ± SD), and (C, F) *Coscinodiscus* sp. (n = 5, ± SD). Gray shaded areas depict moderate light conditions of 95 μmol photons m^{-2} s^{-1}, and white areas depict high-light (HL) exposure at 450 μmol photons m^{-2} s^{-1}. (A–C) Results from nutrient-replete conditions. (D–F) Results under nitrogen depletion. The difference between control and lincomycin treatments reflects PSII repair rate constants (Fig. 4A).

pseudonana, and 3.4×10^7 (± 8.7×10^6) for *Coscinodiscus* sp. During nitrogen starvation, PsbA content of all species decreased (Fig. 2F; Table 2); for *Coscinodiscus*, PsbA dropped below the quantitation limit of 1.2×10^7 $cell^{-1}$. In all cases, the losses of PsbA protein and Chl *a* exceeded the declines expected through growth dilution alone (Table 2). For *E. huxleyi* and *T. pseudonana*, the loss of PsbA was proportional to the loss of Chl *a*. During nitrogen depletion treatments, all species accumulated cellular carbon; in *E. huxleyi*, this process continued over the experimental time span of 38 d.

Functional absorbance cross section for PSII (σ_{PSII})—During exponential growth conditions, σ_{PSII} (± SD, n = 5) of *E. huxleyi* was 3.0 (± 0.3) nm^2 $PSII^{-1}$, *T. pseudonana* was 2.7 (± 0.1) nm^2 $PSII^{-1}$, and *Coscinodicus* sp. was 1.6 (± 0.1) nm^2 $PSII^{-1}$. For all species, σ_{PSII} increased during nitrogen depletion (Fig. 2E). In the case of *E. huxleyi*, σ_{PSII} increased over the first 7 d of nitrogen depletion, but then, as $F_V : F_M$ stabilized so did σ_{PSII}.

ETR (e^- Chl a^{-1} s^{-1}) in *E. huxleyi* and *T. pseudonana* showed no significant changes between nutrient-replete and nitrogen-depleted conditions (Fig. 2G). ETR could not be

estimated for *Coscinodiscus* sp. under nitrogen depletion because of PsbA levels falling below experimental quantitation limits, so we decided not to report any ETR data for *Coscinodiscus* sp.

PSII repair rate constants (R_{PSII}), effective target size for photoinactivation (σ_i), and PSII photoinactivation rates (PSII cell^{-1} s^{-1})—PSII repair rate constants are determined from the difference in $F_V : F_M$ of control and lincomycin treatments (absence of PSII repair, described previously) during high-light challenge experiments at 450 μmol photons m^{-2} s^{-1}, as shown in Fig. 3A–F for all species. Under nutrient-replete conditions, *E. huxleyi* could induce significantly higher PSII repair rate constants than either of the diatom species when subject to an upward fluctuation in light (Fig. 3AC and summarized in Fig. 4A). Under nitrogen depletion, the capacity to rapidly induce PSII repair rates decreased in all three species, although it may have taken *E. huxleyi* almost a week longer to reach the same depressed PSII repair rate constants (Fig. 3D–F and summarized in Fig. 4A). Additionally, under nitrogen depletion, *E. huxleyi* was the only species that retained the capacity to induce significant PSII repair rate constants ($6.9 \pm 3 \times 10^{-5}$ s^{-1}) after transferred from high light back to a moderate light level of 95 μmol photons m^{-2} s^{-1} (Fig. 3D–F).

The effective target size for photoinactivation of PSII (σ_i) is calculated from the decrease in $F_V : F_M$ in relation to cumulative photons in the lincomycin treatment (absence of PSII repair) over 90 min of high-light exposure. Under nutrient-replete conditions, *E. huxleyi* was more susceptible to PSII photoinactivation than were the diatoms (Fig. 4B), but under nitrogen depletion, *E. huxleyi*'s susceptibility to photoinactivation dropped to ~ 25% of the nutrient-replete initial value, whereas the diatoms did not change their susceptibility to photoinactivation of PSII (Fig. 4B) under nitrogen depletion. Figure 5 compares the susceptibility to photoinhibition of all three species under nutrient-replete and nutrient-depleted conditions.

The number of PSII complexes (± SD) that were photoinactivated and therefore needed to be replaced to counter photoinhibition in *E. huxleyi* decreased 21-fold from 32 (± 2.5) cell^{-1} s^{-1} at exponential growth to 1.5 (± 0.2) cell^{-1} s^{-1} during nitrogen depletion through a combination of decreased susceptibility to photoinactivation and lower PSII content per cell under nitrogen depletion. Thus, under nitrogen depletion, *E. huxleyi* maintained an economical PSII repair cycle and retained capacity for PSII repair. For *T. pseudonana*, the number of PSII complexes that needed to be replaced decreased 5-fold, from 20 (± 3.8) cell^{-1} s^{-1} under nutrient-replete growth to 4 (± 1) cell^{-1} s^{-1} under nitrogen depletion (Fig. 4C). In the diatom, this change resulted from the drop in PSII content per cell since susceptibility to photoinactivation did not change. The number of PSII complexes that were photoinactivated and needed to be replaced to counter photoinhibition could not be estimated for *Coscinodiscus* sp. under nitrogen depletion since PsbA levels dropped below experimental quantitation limits.

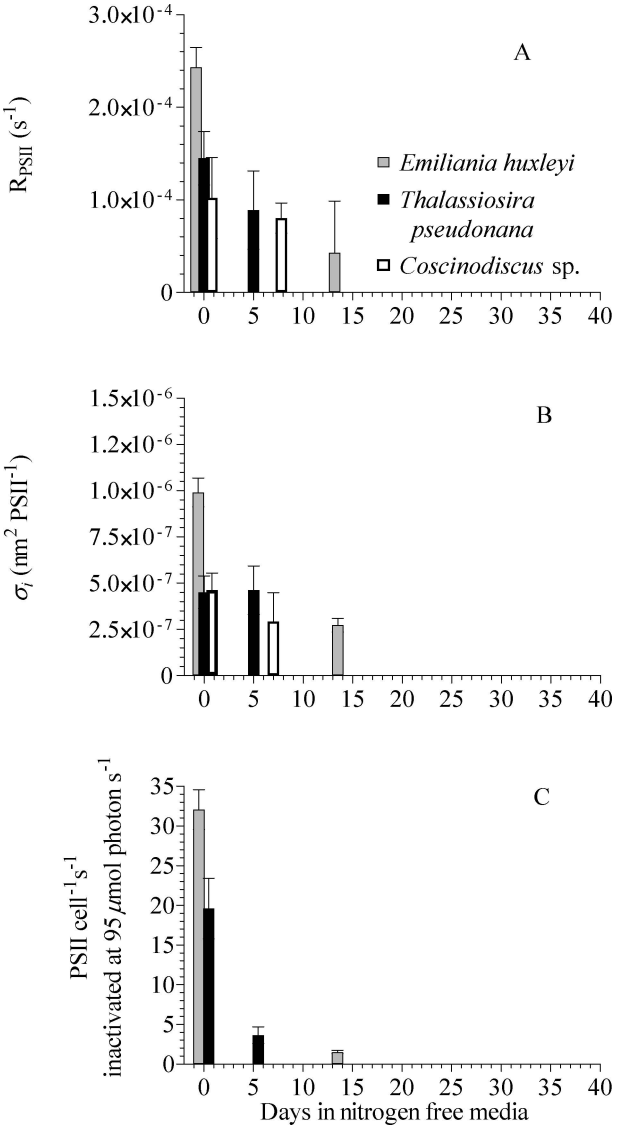

Fig. 4. (A) PSII repair rate constants (s^{-1}) for *E. huxleyi* (n = 4, ± SD), *T. pseudonana* (n = 5, ± SD), and *Coscinodiscus* sp. (n = 5, ± SD). (B) Effective target size for photoinactivation of PSII (σ_i) (nm^2 PSII^{-1}) for *E. huxleyi* (n = 4, ± SD), *T. pseudonana* (n = 5, ± SD), and *Coscinodiscus* sp. (n = 5, ± SD); σ_i values are given in absolute numbers so that higher values indicate a higher susceptibility to photoinactivation. (C) PSII complex photoinactivation (PSII cell^{-1} s^{-1}) at an irradiance of 95 μmol photons m^{-2} s^{-1}, following Eq. 4 for *E. huxleyi* (n = 4, ± SD) and *T. pseudonana* (n = 4, ± SD). The number of PSII complexes that were photoinactivated could not be estimated for *Coscinodiscus* sp. since PsbA protein levels dropped below experimental quantitation limits under nitrogen depletion.

Discussion

We show that *E. huxleyi* can maintain some PSII activity over at least 38 d of nitrogen depletion, as indicated by maintenance of $F_V : F_M$. In contrast, the PSII function in the diatoms *T. pseudonana* and *Coscinodiscus* sp. dropped to marginal levels after 7–10 d. Under phosphorus depletion, PSII function declined sharply within 7 d in *E.*

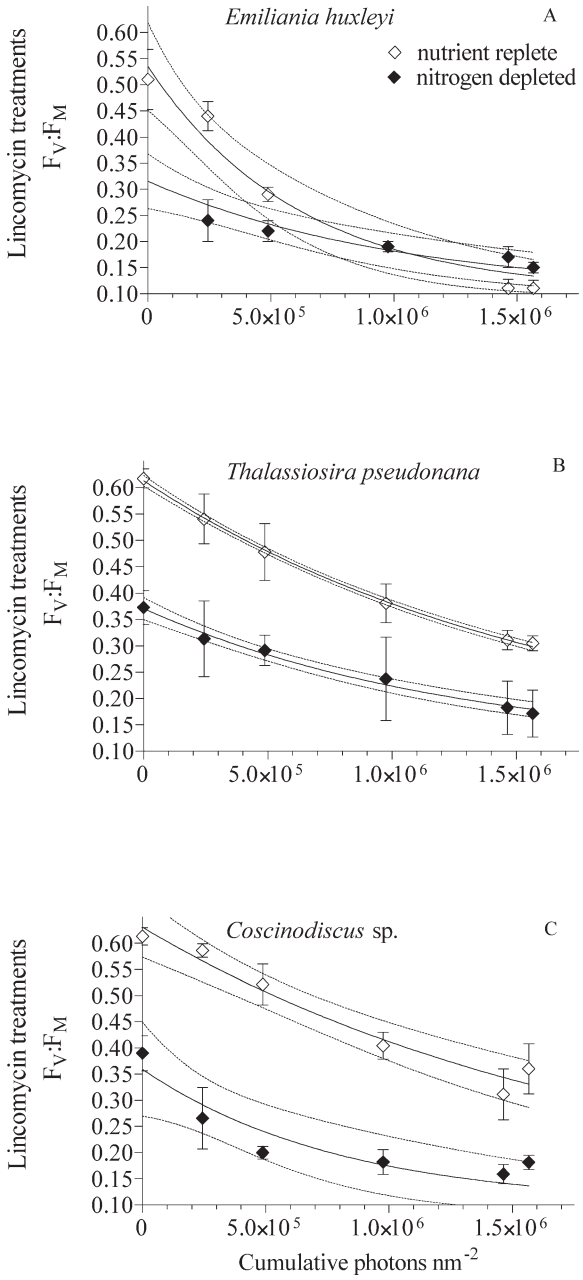

Fig. 5. $F_V : F_M$ plotted vs. cumulative photons applied during lincomycin (absence of PSII repair) light challenge treatments for cells under nutrient-replete conditions (white diamonds) or under nitrogen depletion (black diamonds) for (A) *E. huxleyi* ($n = 4$, ± SD), (B) *T. pseudonana* ($n = 5$, ± SD), and (C) *Coscinodiscus* sp. ($n = 5$, ± SD). In *E. huxleyi*, $F_V : F_M$ under nitrogen depletion declines slowly vs. cumulative photons, compared to nutrient-replete conditions, indicating that the remaining PSII in nitrogen-starved *E. huxleyi* cells are less susceptible to photoinactivation than the PSII in nutrient-replete *E. huxleyi* cells.

huxleyi and within 3 d in *T. pseudonana*, indicating that *E. huxleyi* is adapted to maintain PSII function under long-term nitrogen depletion but not under phosphorus depletion. This capacity of *E. huxleyi* to sustain photosynthetic function under nitrogen-depleted conditions relative to the diatoms may explain its ability to form large blooms under low-nitrogen, high-light conditions.

Under nutrient-replete conditions, *E. huxleyi* had about a 2–2.5-fold higher PSII repair rate constants compared to the two diatoms in this study. Compared to previous studies, *E. huxleyi* had about 2–10-fold higher PSII repair rate constants than *Ostreococcus*, *Pyramimonas obovata* (Prasinophyceae) (Six et al. 2009), *Prochlorococcus*, and *Synechococcus* (Six et al. 2007) and a panel of centric diatoms from the genera *Thalassiosira* and *Coscinodiscus* (Key et al. 2009). These studies used a similar experimental setup to our study, albeit with a lower initial growth light of 30 μmol photons m^{-2} s^{-1}, and no day : night cycle. PSII repair rate constants in our study probably represent a midrange of the possible inducible PSII repair of *E. huxleyi* since Ragni et al. (2008) report that the PSII repair in *E. huxleyi* cells adapted to 300 μmol photons m^{-2} s^{-1} is approximately two times higher than in cells adapted to 30 μmol photons m^{-2} s^{-1}. The large capacity for rapid induction of PSII repair in *E. huxleyi* may be in part responsible for the lack of observed photoinhibition of photosynthesis in this species when exposed to high light (Nanninga and Tyrrell 1996).

PSII repair rate constants under high-light exposure (450 μmol photons m^{-2} s^{-1}) decreased for all species under nitrogen depletion. *E. huxleyi*, however, recovers from high-light stress under nitrogen depletion faster than the investigated diatoms since it was the only species that could induce PSII repair during the recovery phase of the light challenge experiments (Fig. 3D).

The ability of *E. huxleyi* to recover from high light much better than the diatoms might help *E. huxleyi* deal with changing light intensities as they frequently occur in mixed layers. Assuming that the temporal decrease in PSII repair mirrors the more frequently sampled changes in $F_V : F_M$, it takes much longer for PSII repair rates to decrease in *E. huxleyi* when exposed to nitrogen depletion than to phosphorus depletion.

During the first days of nitrogen depletion, the loss of reaction centers exceeded the loss of antenna complexes as indicated by an increasing functional absorbance cross section of PSII (σ_{PSII}) (Fig. 2E) and increasing Chl *a* : PsbA ratios in all species (Table 2). D1 protein (PsbA) content is a molecular proxy for the content of PSII reaction centers (Burns et al. 2006). The increase in σ_{PSII} means that the remaining PSII centers are performing photochemical charge separations at a faster rate per center under the growth light level. In addition, *E. huxleyi* counterbalanced lower PSII repair with a lowered susceptibility to PSII photoinactivation (σ_i) under nitrogen-depleted conditions. In contrast, the susceptibility to photoinactivation in diatoms did not change under nutrient depletion. Both σ_{PSII} and σ_i are target size parameterizations with units of area, and the ratio of $\sigma_{PSII} : \sigma_i$ gives the ratio of PSII photochemical charge separations to PSII photoinactivations. In *T. pseudonana* under growth conditions, $\sigma_{PSII} : \sigma_i = 5.6 \times 10^6$ photochemical charge separations per PSII photoinactivation event. Under nitrogen depletion, this ratio increases to 8.0×10^6, indicating a somewhat longer functional life of PSII before photoinactivation. In marked

contrast, in *E. huxleyi* under growth conditions, $\sigma_{PSII} : \sigma_i$ is only 3×10^6, commensurate with the rapid PSII repair rates necessary to maintain PSII function. Under nitrogen depletion, however, in *E. huxleyi*, $\sigma_{PSII} : \sigma_i$ increases sharply to 1.6×10^7, a 5-fold increase in the number of PSII photochemical duty cycles per photoinactivation event. Therefore, the PSII repair cycle becomes economical under nitrogen depletion in *E. huxleyi*, accounting for the capacity of *E. huxleyi* to maintain PSII function under nitrogen depletion and providing a mechanistic explanation for the prevalence of *E. huxleyi* blooms under high-light, low-nitrogen conditions, often following diatom blooms (Tyrrell and Merico 2004).

It remains unexplained how *E. huxleyi* achieves a drop of ~ 75% in susceptibility to PSII photoinactivation under nitrogen depletion. We speculate that enhanced production of dimethylsulfoniopropionate (DMSP) might be involved. The similarity in structure and properties between DMSP and glycine betaine lead to the hypothesis that DMSP could act as an osmolyte and replace nitrogen-containing glycine betaine under nitrogen limitation (Challenger 1951). *E. huxleyi* produces DMSP (Keller et al. 1999), which had been proposed as the first link of an antioxidant system in marine algae that reacts rapidly with the hydroxyl radical (·OH). Moreover, the DMSP enzymatic cleavage products, dimethyl sulfide (DMS) and acrylate, are even more effective at scavenging ·OH (Sunda et al. 2002). *E. huxleyi*'s intracellular DMSP concentration is indeed inversely related with nitrogen-limited growth rates (Keller et al. 1999), whereas phosphorus limitation had no effect on DMSP production (Wilson et al. 1998), consistent with our contrasting results of *E. huxleyi* maintaining PSII function for a long period under nitrogen depletion but only short term under phosphorus depletion (Fig. 1A,B). In nitrogen-depleted *E. huxleyi* cultures, we noted the strong, characteristic odor of DMS, a breakdown product of DMSP. *T. pseudonana* also increases intracellular DMSP concentration during nitrogen- or phosphorus-limited growth (Bucciarelli and Sunda 2003), so the question arises as to whether DMSP induction might also decrease the susceptibility to photoinactivation of *T. pseudonana* and why it would be less effective than in *E. huxleyi*.

Our results verify our hypothesis that *E. huxleyi* has photophysiological advantages compared to the examined diatoms. Under nutrient-replete conditions, *E. huxleyi* has one of the highest PSII repair rate constants among phytoplankton examined to date (this study; Ragni et al. 2008). Under nitrogen depletion, *E. huxleyi* maintains basal PSII activity for much longer periods than the examined diatom species as reflected by the fluorescence-based maximum quantum yields as well as by ongoing accumulation of cellular carbon. *E. huxleyi* increases photoprotection under nitrogen-depleted conditions, perhaps using a sulfur-based pathway. Additionally, after induced high-light stress under nutrient depletion, PSII repair rates at moderate light levels are sufficient in *E. huxleyi* to regain a moderate PSII function, which is not the case in the diatoms. Whereas high PSII repair rate constants could support *E. huxleyi* at the onset of a bloom when nitrogen is still available and the water column becomes stratified, lowered PSII photoinactivation under nitrogen depletion might prolong bloom duration. In contrast, phosphorus depletion affects photosystem II function in *E. huxleyi* much earlier than does nitrogen depletion, indicating that *E. huxleyi* blooms may terminate sooner in low-phosphorus, high-N : P waters than in low-nitrogen, low-N : P waters.

Acknowledgments

We thank Björn Rost (Alfred Wegener Institute for Polar and Marine Research, Germany) for providing *E. huxleyi* cultures and Laurel McIntyre for providing *Coscinodiscus* sp. (CCMP 1583) cultures. We are grateful to Mary Beth Bissell, Jillian Greene, and Sarah Tulk for protein detections. Ruby Hu gave helpful lab assistance. Andy Spring and Cindy Spicer performed carbon-nitrogen analyses. The work was funded by the Natural Sciences and Engineering Research Council of Canada (ZF, DC), the Canadian Foundation for Innovation (ZF, DC), and the New Brunswick Innovation Foundation (ZF, AC). Two anonymous reviewers gave helpful and constructive comments which improved the manuscript.

References

Allakhverdiev, S., and N. Murata. 2004. Environmental stress inhibits the synthesis de novo of proteins involved in the photodamage–repair cycle of photosystem II in *Synechocystis* sp. PCC 6803. BBA-Bioenerg. **1657:** 23–32.

Bachmann, K. M., V. Ebbert, W. W. Adams, A. S. Verhoeven, B. A. Logan, and B. Demmig-Adams. 2004. Effects of lincomycin on PSII efficiency, non-photochemical quenching, D1 protein and xanthophyll cycle during photoinhibition and recovery. Funct. Plant Biol. **31:** 803–813, doi:10.1071/FP04022

Berges, J. A., D. J. Franklin, and P. J. Harrison. 2001. Evolution of an artificial seawater medium: Improvements in enriched seawater, artificial water over the last two decades. J. Phycol. **37:** 1138–1145, doi:10.1046/j.1529-8817.2001.01052.x

Bucciarelli, E., and W. G. Sunda. 2003. Influence of CO_2, nitrate, phosphate, and silicate limitation on intracellular dimethylsulfoniopropionate in batch cultures of the coastal diatom *Thalassiosira pseudonana*. Limnol. Oceanogr. **48:** 2256–2265, doi:10.4319/lo.2003.48.6.2256

Burns, R., T. Mackenzie, and D. Campbell. 2006. Inorganic carbon repletion constrains steady-state light acclimation in the cyanobacterium *Synechococcus elongatus*. J. Phycol. **42:** 610, doi:10.1111/j.1529-8817.2006.00220.x

Challenger, F. 1951. Biological methylation. Adv. Enzymol. **12:** 429–491.

Egge, J. K., and B. R. Heimdal. 1994. Blooms of phytoplankton including *Emiliania huxleyi* (Haptophyta): Effects of nutrient supply in different N:P ratios. Sarsia **79:** 333–348.

Falkowski, P., and Z. Kolber. 1995. Variations in chlorophyll fluorescence yields in phytoplankton in the world oceans. Aust. J. Plant Phys. **22:** 341–355, doi:10.1071/PP9950341

Hakala, M., I. Tuominen, M. Keranen, T. Tyystjarvi, and E. Tyystjarvi. 2005. Evidence for the role of the oxygen-evolving manganese complex in photoinhibition of photosystem II. Biochim. Biophys. Acta **1706:** 68–80, doi:10.1016/j.bbabio.2004.09.001

Holligan, P. E., and others. 1993. A biogeochemical study of the coccolithophore, *Emiliania huxleyi*, in the North Atlantic. Glob. Biogeochem. Cycles **7:** 879–900, doi:10.1029/93GB01731

Iglesias-Rodríguez, M. D., and others. 2002. Representing key phytoplankton functional groups in ocean carbon cycle models: Coccolithophorids. Glob. Biogeochem. Cycles **16:** 1100, doi:10.1029/2001GB001454

Jeffrey, S. W., and G. F. Humphrey. 1975. New spectrophotometric equations for determining chlorophylls a, b, c1 and c2 in higher plants, algae, and natural phytoplankton. Biochem. Physiol. Pflanz. **167:** 191–194.

Keller, M., R. Kiene, P. Matrai, and W. Bellows. 1999. Production of glycine betaine and dimethylsulfoniopropionate in marine phytoplankton. I. Batch cultures. Mar. Biol. **135:** 237–248.

Key, T., A. McCarthy, D. A. Campbell, C. Six, S. Roy, and Z. V. Finkel. 2009. Cell size trade-offs govern light exploitation strategies in marine phytoplankton. Environ. Microbiol. **12:** 95–104, doi:10.1111/j.1462-2920.2009.02046.x

Lessard, E. J., A. Merico, and T. Tyrrell. 2005. Nitrate: Phosphate ratios and *Emiliania huxleyi* blooms. Limnol. Oceanogr. **50:** 1020–1024, doi:10.4319/lo.2005.50.3.1020

Nanninga, H., and T. Tyrrell. 1996. Importance of light for the formation of algal blooms by *Emiliania huxleyi*. Mar. Ecol. Prog. Ser. **136:** 195–203, doi:10.3354/meps136195

Nishiyama, Y., S. Allakhverdiev, and N. Murata. 2006. A new paradigm for the action of reactive oxygen species in the photoinhibition of photosystem II. BBA-Bioenerg. **1757:** 742–749.

Oguz, T., and A. Merico. 2006. Factors controlling the summer *Emiliania huxleyi* bloom in the Black Sea: A modeling study. J. Mar. Sys. **59:** 173–188, doi:10.1016/j.jmarsys.2005.08.002

Paasche, E. 2002. A review of the coccolithophorid *Emiliania huxleyi*. Phycologia **40:** 503–529, doi:10.2216/i0031-8884-40-6-503.1

Palenik, B., and S. Henson. 1997. The use of amides and other organic nitrogen sources by the phytoplankton *Emiliania huxleyi*. Limnol. Oceanogr. **42:** 1544–1551, doi:10.4319/lo.1997.42.7.1544

Parkhill, J., G. Maillet, and J. Cullen. 2001. Fluorescence-based maximal quantum yield for PSII as a diagnostic of nutrient stress. J. Phycol. **37:** 517–529, doi:10.1046/j.1529-8817.2001.037004517.x

Ragni, M., R. Airs, N. Leonardos, and R. Geider. 2008. Photoinhibition of PSII in *Emiliania huxleyi* (Haptophyta) under high light stress: The roles of photoacclimation, photoprotection, and photorepair. J. Phycol. **44:** 670–683, doi:10.1111/j.1529-8817.2008.00524.x

Raitsos, D. E., S. J. Lavender, Y. Pradhan, T. Tyrrell, P. C. Reid, and M. Edwards. 2006. Coccolithophore bloom size variation in response to the regional environment of the Subarctic North Atlantic. Limnol. Oceanogr. **51:** 2122–2130, doi:10.4319/lo.2006.51.5.2122

Riegman, R., A. A. M. Noordeloos, and G. C. Cadée. 1992. *Phaeocystis* blooms and eutrophication of the continental coastal zones of the North Sea. Mar. Biol. **112:** 479–484, doi:10.1007/BF00356293

———, W. Stolte, A. A. M. Noordeloos, and D. Slezak. 2000. Nutrient uptake and alkaline phosphatase (EC 3:1:3:1) activity of *Emiliania huxleyi* (Prymnesiophyceae) during growth under N and P limitation in continuous cultures. J. Phycol. **36:** 10, doi:10.1046/j.1529-8817.2000.99023.x

Sciandra, A., J. Harlay, D. Levèvre, R. Lemée, P. Rimmelin, M. Denis, and J.-P. Gattuso. 2003. Response of coccolithophorid *Emiliania huxleyi* to elevated partial pressure of CO_2 under nitrogen limitation. Mar. Ecol Prog. Ser. **261:** 111–122, doi:10.3354/meps261111

Six, C., Z. V. Finkel, A. J. Irwin, and D. A. Campbell. 2007. Light variability illuminates niche-partitioning among marine picocyanobacteria. PLoS ONE **2:** e1341, doi:10.1371/journal.pone.0001341

———, ———, F. Rodriguez, D. Marie, F. Partensky, and D. Campbell. 2008. Contrasting photoacclimation costs in ecotypes of the marine eukaryotic picoplankter *Ostreococcus*. Limnol. Oceanogr. **53:** 255–265.

———, R. Sherrard, M. Lionard, S. Roy, and D. Campbell. 2009. Photosystem II and pigment dynamics among ecotypes of the green alga *Ostreococcus*. Plant Physiol. **113:** 379–390, doi:10.1104/pp.109.140566

Strom, S. L., and K. L. Bright. 2009. Inter-strain differences in nitrogen use by the coccolithophore *Emiliania huxleyi*, and consequences for predation by a planktonic ciliate. Harmful Algae **8:** 811–816, doi:10.1016/j.hal.2007.10.005

Sunda, W., D. J. Kieber, R. P. Kiene, and S. Huntsman. 2002. An antioxidant function for DMSP and DMS in marine algae. Nature. **418:** 317–320, doi:10.1038/nature00851

Tyrrell, T., and A. Merico. 2004. *Emiliania huxleyi*: Bloom observations and the conditions that induce them, p. 75–97. *In* H. R. Thierstein and J. R. Young [eds.], Coccolithophores: From molecular processes to global impact. Springer.

———, and A. Taylor. 1996. A modelling study of *Emiliania huxleyi* in the NE Atlantic. J. Mar. Sys. **9:** 83–112, doi:10.1016/0924-7963(96)00019-X

Tyystjarvi, E., and E. M. Aro. 1996. The rate constant of photoinhibition, measured in lincomycin treated leaves, is directly proportional to light intensity. Proc. Natl. Acad. Sci. USA **93:** 2213–2218, doi:10.1073/pnas.93.5.2213

Wilson, W., S. Turner, and N. Mann. 1998. Population dynamics of phytoplankton and viruses in a phosphate-limited mesocosm and their effect on DMSP and DMS production. Estuar. Coast. Shelf Sci. **46:** 49–59, doi:10.1006/ecss.1998.0333

Associate editor: Heidi M. Sosik

Received: 11 December 2009
Accepted: 26 March 2010
Amended: 31 May 2010